

# Effect of structure configurations and wind characteristics on the design of solar concentrator support structure under dynamic wind action

Bassem Kaabia\*, Sébastien Langlois<sup>a</sup> and Sébastien Maheux<sup>b</sup>

Department of Civil Engineering, Université de Sherbrooke, 2500 boul. de l'Université, Sherbrooke, QC, Canada, J1K2R1

(Received June 19, 2017, Revised March 1, 2018, Accepted March 6, 2018)

**Abstract.** Concentrated Solar Photovoltaic (CPV) is a promising alternative to conventional solar structures. These solar tracking structures need to be optimized to be competitive against other types of energy production. In particular, the selection of the structural parameters needs to be optimized with regards to the dynamic wind response. This study aims to evaluate the effect of the main structural parameters, as selected in the preliminary design phase, on the wind response and then on the weight of the steel support structure. A parametric study has been performed where parameters influencing dynamic wind response are varied. The study is performed using a semi-deterministic time-domain wind analysis method. Unsteady aerodynamic model is applied for the shape of the CPV structure collector at different configurations in conjunction with a consistent mass-spring-damper model with the corresponding degrees of freedom to describe the dynamic response of the system. It is shown that, unlike the static response analysis, the variation of the peak wind response with many structural parameters is highly nonlinear because of the dynamic wind action. A steel structural optimization process reveals that close attention to structural and site wind parameters could lead to optimal design of CPV steel support structure.

**Keywords:** solar concentrator structure; finite element analysis; wind simulation; dynamic effect; wind load optimization

## 1. Introduction

Structural optimization of solar trackers under wind load is one of the key parameters in order to get the lowest cost of energy (LCOE). Indeed, the steel support structure could account approximately for more than 30% of the total cost (Wu *et al.* 2014). Moreover, wind conditions, in addition to annual insolation, should be considered to determine if operation at specific locations might be affected significantly by winds (Randall 1983). At present, limited guidelines on the design of solar ground-mounted structures are available. Most of the previous research work are based on wind tunnel test investigation. The large studies of the National Renewable Energy Laboratory (NREL) (Peterka *et al.* 1980, Hosoya *et al.* 2008), the Solar Energy Research Institute (SERI) (Murphy 1981) and the Energy and Environment (ENEA) (Salomoni *et al.* 2009, Giannuzzi *et al.* 2007) are recognized to improve the understanding of the specific design objective for these special structures under wind load. However, more quantitative numerical studies are needed in order to get conclusive and general tools to evaluate wind load on solar structure in a preliminary design context. It is also essential to take into consideration the dynamic wind action effect to achieve a more reliable wind load evaluation (Banks 2012).

Many of the wind load optimization studies are recently oriented to the Computational Fluid Dynamic (CFD) in order to optimize the aerodynamic forces applied to the

principal structural members (Fu *et al.* 2015, Gil *et al.* 2009). However, the huge computational time and the complexity of the CFD models make also the integration of the results in a dynamic structural analysis extremely difficult. Yet, little work has been devoted to investigate the time-domain response of this type of structure under turbulent wind by introducing the adequate aerodynamic model and the dynamic characteristics of the system in a dynamic structural analysis. However, many studies were conducted for conventional structures such as Letchford *et al.* (1993) for low rise buildings, Chen and Kareem (2002) for long-span bridges and Gani and Légéron (2010) for guyed tower structures. Then, it is important to be inspired from these precedent studies and to pay a special attention to the analysis hypotheses to be used specifically for solar structures before being involved in extended parametric studies. In this context, Zlatanov and Weinrebe (2013) used the finite element method in conjunction with structural model to optimize support structure for arbitrary tracker geometries under known wind conditions. However, less attention is paid to highlight the dynamic effect induced by wind action.

The main objective of this study is to evaluate the effect of principal pre-design structural parameters and the site environment characteristics on the peak wind response and then on the weight of the steel support structure based on advanced wind analysis methods applied to a parametrized and a generic finite element model. The utility of this study derives from performing a mapping of structural parameters to be related to steel structure costs and to be useful for a preliminary design decision for this type of structure in general. The current work is based on a reference full-scale measurement of a CPV prototype installed in Sherbrooke,

---

\*Corresponding author, Ph.D.

E-mail: Bassem.Kaabia@usherbrooke.ca

Canada (Kaabia *et al.* 2017a). The experimental results helped to develop a semi-deterministic time domain wind analysis method predicting coherently the statistical parameters of the wind response with acceptable discrepancies (Kaabia *et al.* 2017b).

The benchmark prototype studied in this paper could be classified with two-axes isolated solar tracker with large exposed surface and a relatively small focal ratio  $f/D$ . This type of tracking structure is generally composed of large reflector surface supported by a spatial truss structure. Depending on the exposed area to wind, aspect ratio, weight and flexibility of the steel support structure, the total response is differently affected by the wind action for various configurations at specific site conditions. Therefore, a thorough investigation of the influence of these parameters on the support structure steel weight to withstand the induced wind action is recommended. Economic zones could be highlighted in a preliminary design phase in function of the correlation of many wind and structural parameters. Potential solutions for cost-effective structural design could then be studied.

In this paper, the methodology of the developed numerical wind analysis tool based on the simplified parametric model and the methodology of the parametric study are explained. The results are exposed in two parts. First, the validation of the time-domain analysis method is presented in comparison to the full-scale experimental results and the implemented frequency domain approach. Second, the results of the parametric study including structural, geometric and wind parameters are presented, and the preliminary design phase recommendations are underlined.

## 2. Methodology

### 2.1 CPV prototype and measurement

The studied CPV prototype is a 35 kW tracker that uses 128 identical reflective solar panels spreading on a  $16 \times 8 \text{ m}^2$  surface. The steel structure is composed of three principal parts. The panels are held on a parabolic frame that uses 32 identical steel lattice trusses. The Dense Receiver Array (DRA) is supported by a double guyed mast. These elements are all mounted on a two-axis tracker base that points the solar concentrator precisely towards the sun throughout the day. The elevation rotation of the reflector dish around a HSS 200x200 central beam is assured by two mechanical actuators. The azimuthal control is assured by the azimuth motor drive which is fixed to the ground. The total weight of the CPV prototype is approximately 135.4 kN in which 108.0 kN are coming from the steel structure. The base tower steel weight is approximately equal to 37.0 kN. A36 steel with elastic limit of 250 MPa is typically used for this prototype (Fig. 1(a)).

Twelve Linear Variable Differential Transformer (LVDT) sensors were installed on the structure. They were attached by pairs to each of the six main tower members. Compression and tensile forces are calculated from the displacement for each members. The current measurement

configuration permitted to measure a global instantaneous base moment in the along wind direction (Figs. 1(b) and 1(c)). Simultaneously, wind characteristics were measured through anemometers. Three of them are fixed at the top of three meteorological towers at a 10 m height. The fourth is fixed at 7.5 m in the middle reference towers, which is distant at approximately 28 m from the center point of the prototype. The recorded data were treated by 10 min samples with sampling rate of 20 Hz. The measurements were taken in different pitch angle  $\gamma$  and different wind characteristics. In this paper only the configurations in which wind direction is perpendicular to the normal axis of the dish collector were analyzed (see Fig. 1(b)). Only along-wind action is considered in calculating the global moment. The moment around the Z axis (global torsion of the structure) could not be evaluated using the measurement configuration. The methodology and the hypotheses for calculating the base moment wind response and the results of the full-scale investigation are detailed in Kaabia *et al.* (2017a).

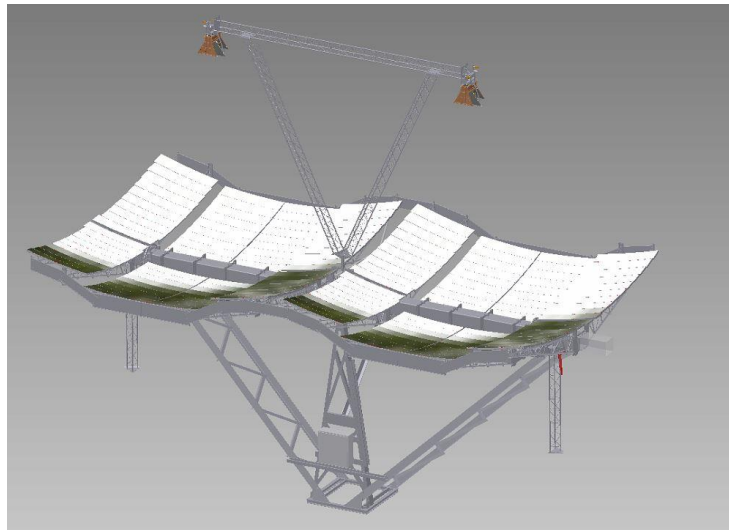
### 2.2 Time-domain wind analysis tool

A finite element model of the solar concentrator steel support structure was developed and time-domain dynamic (TD) analyses were performed. Newmark direct integration scheme with coefficients  $\beta = 0.25$ ,  $\alpha = 0.5$  was used for the time-domain analysis. An aerodynamic force model based on the indicial response function (IRF) associated to the aerodynamic admittance function for the flat plate is used for TD analyses at different configurations. The developed finite element model used for this analysis and the wind force modeling are discussed in the following subsections.

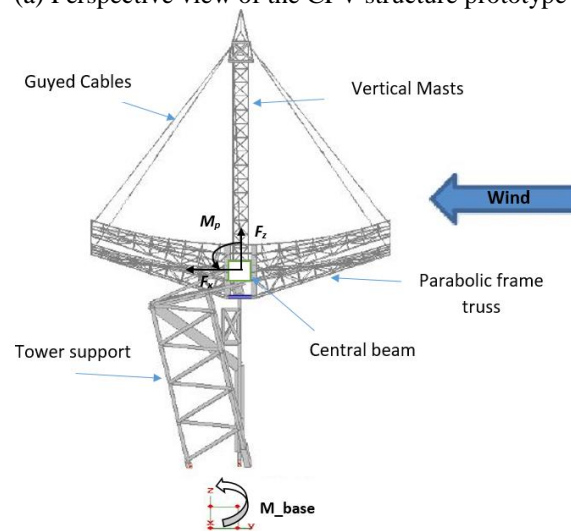
#### 2.2.1 Finite element model

Accurate numerical evaluation of wind response is a key factor to optimize wind action. The main step is to be able to elaborate a simplified structural model, which predicts coherently the total structural behavior of the complete structure in order to approach the characteristics of the dynamic response under wind loads. The utility of simplifying the structural model derives from the flexibility to analyse, with a reasonable computing time, multiple CPV prototype configurations by varying many structural parameters. Then, it could be easily integrated in a preliminary design tool for this type of structure. The modeling study was based on the technical drawings and full 3D CAD model (Fig. 1). For this purpose, Salome-Meca, an open-source simulation platform relying on the finite element solver Code\_Aster, was used.

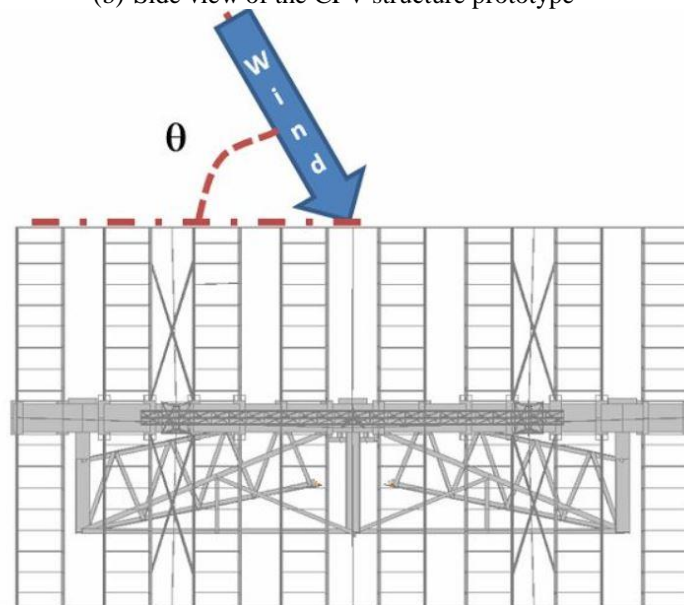
The initial model of the CPV prototype is a complete model that incorporates all parts of the structure except the mirrors and the mechanical drive components. Then, two models were developed in order to get the optimal modeling alternative to be used for the parametric study investigation. First, an intermediate model, which include all the members of the support tower structure model was developed. This model assumes that the rest of the structure (parabolic frame and mast) could behave like a rigid body and then it could be replaced by discrete mass and mass moment of



(a) Perspective view of the CPV structure prototype

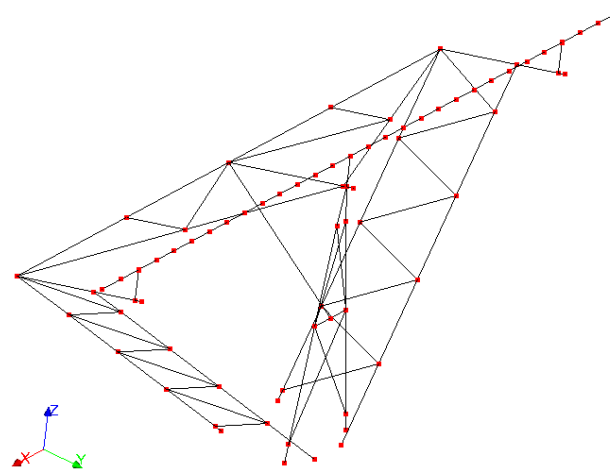


(b) Side view of the CPV structure prototype

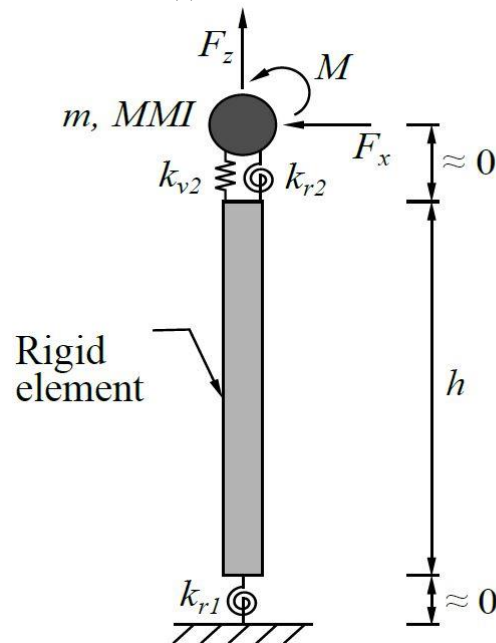


(c) Plan view of the CPV structure prototype

Fig. 1 CPV 3D CAD model in different view (Norman and de St. Croix, 2010)



(a) Intermediate model



(b) Simplified 3-DOF model

Fig. 2 Structural models

inertia concentrated along the central beam (Fig. 2(a)). Second, a much simplified and parametrized model for this structure, which is consistent with the study objective, was developed (Fig. 2(b)). It is shown that large parametric analysis and simulations problem of complex structural system require simple substitute model with reduced degree of freedom, which could give acceptable results compared to complete and intermediate modeling approaches. The most important requirement for this model is to be consistent with the dynamic properties of the complex real system. The required parameters to be identified for the simplified model are the total mass  $m$  and the moment mass of inertia  $MMI$  of the dish which present the effective dynamic for the system. The rotational stiffness of the dish frame including the elevation drive system between the top of the tower and the dish frame is presented by a discrete

rigidity element  $k_{r2}$ . The translational vertical and lateral stiffness is represented by discrete stiffness elements  $k_{v2}$  and  $k_{r1}$ , respectively. The stiffness  $k_{r2}$  is an equivalent rotational stiffness element to replace the swaying stiffness of support tower structure. The modeled rigid element with the height  $h$  allows transferring the aerodynamic forces and moment applied at the central beam level to the structure base. The zero length elements served to define 'SEG' elements instead of nodes in order to get the appropriate representation of the rigidity matrix in Code\_Aster.

A modal analysis was conducted in order to validate the dynamic behavior of the simplified model compared to the intermediate tower support model. The modal analysis shows that the pitching, the swaying and the vertical modes could be found at the frequencies of 1.0, 3.8 and 9.8 Hz, respectively. The pitching and swaying frequencies also

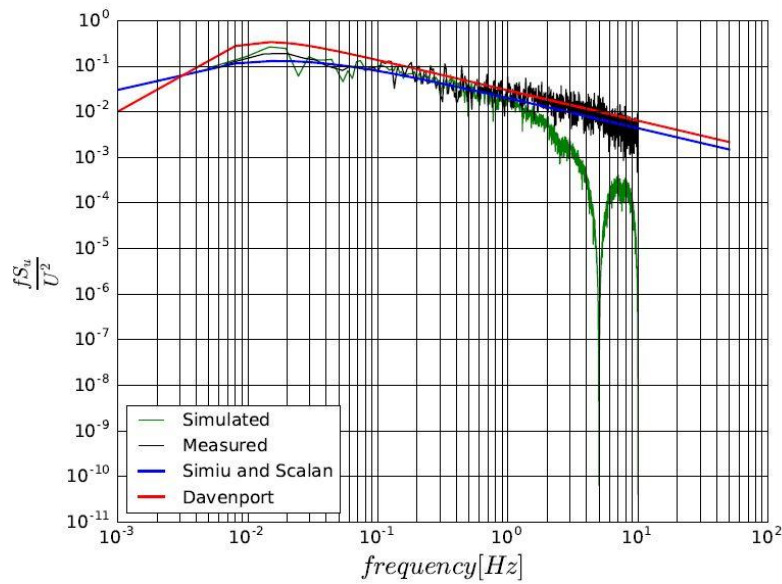


Fig. 3 Typical measured and simulated wind sample spectrum compared to different design empirical spectrum

match the measured values and it is shown that they are associated to coupled modes. A rotation in discrete element at the level  $h$  could lead to simultaneous swaying translation in the along wind direction. The translational stiffness in the X direction was replaced by an equivalent rotational rigidity at the base in order to consider the dependence of the two mode shapes as well as proper presentation of a probable global nonlinear behavior of the structure at its base.

### 2.2.2 Wind loading

The developed numerical model tool can be analyzed with measured wind samples in order to validate full-scale measurements. However, in order to extend the analysis for wind design conditions, it is essential to simulate and generate wind signals for specific site conditions. Spectral stochastic methods are by definition a tool devoted to generate wind samples with different characteristics, depending on the location and the site exposure category, and following design spectrum empirical model. Numerically generated wind samples were obtained for different turbulence intensity  $I_u$ , using the in-house WindGen program developed by (Hang and Légéron 2005) based on the Power Spectral Density (PSD) proposed by Simiu for along wind component using Eq. (1). It is to be noted that WindGen generates only turbulent part of wind speed  $u(z, t)$  which must be combined with mean wind speed  $U$ . Fig. 3 shows the comparison between simulated and analytical wind spectrum.

$$\frac{n S_u(z, n)}{U_*^2} = \frac{200 \frac{nz}{U}}{(1 + 50 \frac{nz}{U})^{5/3}} \quad (1)$$

Where  $n$  is the frequency,  $u^*$  is the shear velocity,  $z$  is the height and  $S_u$  is the power spectrum density (PSD) for the fluctuating wind speed  $u(z, t)$ . The simulation parameters are defined based on the target turbulence and wind speed.

The cut frequency  $\omega_u$  is fixed to 15.73 rad/s in order to guarantee a time step of  $\pi/\omega_u = 0.2$  s.

In general, it is conventional to separate the total along wind force into buffeting and self-excited force. In this paper, it is assumed that the most important component is related to the buffeting forces and additional aerodynamic damping was introduced using the quasi-steady approach (Kaabia *et al.* 2017b). The generated wind speed was then applied to the finite element model as a time-varying loading using Eqs. (3)-(6). The lift and moment aerodynamic coefficients used here were evaluated from wind tunnel measurements made by Gani *et al.* (2011) and the drag force coefficients were evaluated from full-scale measurement for each test sample. In addition, as shown in Kaabia *et al.* (2017b), the use of the quasi-steady approach in modeling fluctuating forces highly overestimates the dynamic response of this type of structure. Then, in order to get more accurate results, refined aerodynamic model was introduced based on the aerodynamic admittance concept. It is found that the plate is the form, among those for which the experimental aerodynamic admittance were evaluated in the past (Davenport 1967, Vickery 1968), that comes closest to the studied parabolic dish geometry. This is especially true for dishes with small focal ratio  $f/D$ . Furthermore, the comparison between measured and calculated forces at the base of the solar structures in Kaabia *et al.* (2017b) showed that the use of the admittance function of a plate could provide adequate results for this particular type of structure studied. The aerodynamic admittance function of a plate that was used of a plate (Vickery 1968) is given as follows

$$\chi_a^2(n) = \frac{1}{1 + 2\pi^2 \sqrt{nA/U}} \quad (2)$$

In time-domain, the equivalent indicial response function used in this study is based on the procedure presented in Chang (2010) based on the work of Scanlan (1993). As an example, the along wind force applied at the level  $h$  (central beam) is

calculated as follows

$$F(t) = \bar{F} + f(t) \quad (3)$$

$$f(t) = \rho_{air} U A C_{fx} \int_0^s [u(s) - \varphi'(s - \sigma)] d\sigma \quad (4)$$

$$\bar{F} = \frac{1}{2} \rho_{air} A C_{fx} U^2 \quad (5)$$

$$\varphi' = 0.075e^{-0.513s} + 1.794e^{-2.111s} \quad (6)$$

$$s = Ut/\sqrt{A} \quad (7)$$

where  $F(t)$  is the drag force linearized to be composed of the mean force component  $\bar{F}$  and the turbulent component  $f(t)$ .  $\rho_{air}$  is the density of air for a reference temperature,  $A$  is the total dish collector area,  $C_{fx}$  is the force coefficient along the X axis,  $\varphi'$  is the derivative of indicial function  $\varphi$  for flat plate,  $s$  is the nondimensional time. The lift force and the pitching moment were calculated using the same process.

### 2.3 Definition of dynamic parameters

In this paper, the target parameter to be studied is the overturning base moment  $M$  (Fig. 1). It is always possible to compare the deterministic time domain results to the stochastic dynamic parameters in term of maximum moment  $M_{max}$ , standard deviation  $s$  and response peak factor  $g$  values. Assuming that wind speed and consequently wind response are stationary random series following the normal stochastic law (Davenport 1961), the peak moment response value could be related to the other parameters by the key statistical formulation

$$M_{max} = M + g \sigma \quad (8)$$

The gust effect factor  $GEF$  is a key concept which provides a suitable reference tool for the calculation of the dynamic response quantities due to a longitudinal gust force. It could be then used as reference parameter for comparison between the time-domain method, Davenport's spectral approach in its basic form (Davenport 1961) and the ASCE 7-10 S(ASCE7-10, 2010). The  $GEF$  in its deterministic and stochastic formulations was evaluated for the time-domain and the stochastic spectral approach using Eqs. (9) and (10), respectively.

$$GEF = \frac{M_{max}/M}{G_v^2} \quad (9)$$

$$GEF = \frac{1 + g\sigma\bar{M}}{G_v^2} \quad (10)$$

where  $G_v$  is the wind gust factor based on 3-s gust duration as used in ASCE 7-10.

The ASCE7-10 was adapted and applied to calculate the key wind response parameters for this type of structure by considering only the first pitching mode as shown in Kaabia *et al.* (2017a). Davenport's spectral approach in its basic form (Davenport 1961) was applied using the admittance function for the flat plate and considering the narrow band assumption for the resonance component calculation. It is considered that the along-wind maximum response is coming from the pitching moment  $M_p$  and the drag force  $F_x$ . Theoretically, The peak value of  $M_p$  and  $F_x$  do not occur at the same time because they are caused by different flow conditions. Then, it was calculated using the square-root-of-sum-of-squares (SRSS) combination method. The algebraic combination method was also further tested for the application of both the spectral approach and the ASCE 7-10 in the parametric study results.

### 2.4 Parametric study and study case definition

In the following, the geometry of the tracker, including area size and the aspect ratio, the structural parameters, including lateral and rotational rigidity and the damping, and the wind characteristics were parameterized. The effective dynamic mass was assumed to be proportional to the total dish area for simplification. The tracker height above ground and the initial geometric configurations of the support tower were not changed during the entire study. The following parameters grid was tested and more than 284 configurations were investigated using the 3-DOF model. 10 wind signals were used for each configuration test in order to evaluate average values. The benchmark reference prototype parameters are highlighted in bold. Site specific design wind speed were selected based on the 3-s wind speed maps of the ASCE7-10 for different reference locations in the USA.

- Dish area [m<sup>2</sup>] : 10,20,30,40,50,60,70,80,90,100,110,**120**,130,140,150,160;
- Aspect ratio [-] : 1.0, **1.8**,2.5;
- Pitch angle [°] : 0,45,30,60,**90**;
- Pitching frequency [Hz] : 0.4,0.6,0.8,**1.0**,1.2,1.4,1.6;
- Swaying frequency [Hz] : 1.6,2.3,3.1,**3.8**,4.6,5.3;
- Damping ratio [-] : **0.025**,0.05,0.075,0.1,0.2;
- Mean wind speed [m/s<sup>2</sup>] : 10,20,**30**,40,50,60,70,80,90;
- Turbulence intensity [%] : 13,18,27,**30**,35,40;
- Design wind speed per location [m/s<sup>2</sup>] : **45**,55,75,85;
- Site category(Turbulence intensity[%]) : A(40),**B(30)**,C(18),D(13);

## 3. Results and discussions

### 3.1 Validation of wind load analysis

The results of the CPV simulated wind response are compared to the experimental full-scale measured wind response in term of mean, maximum and standard deviation

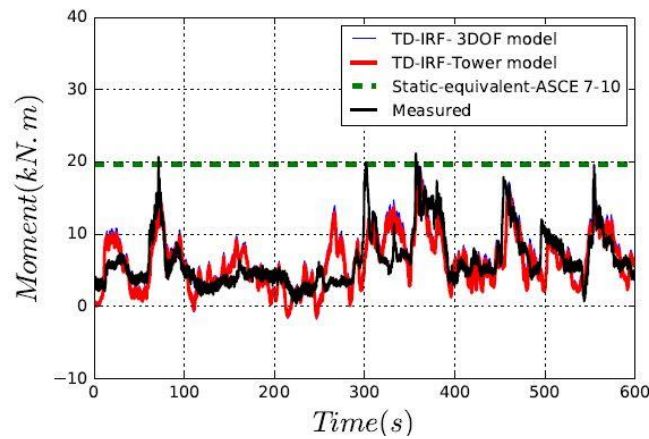
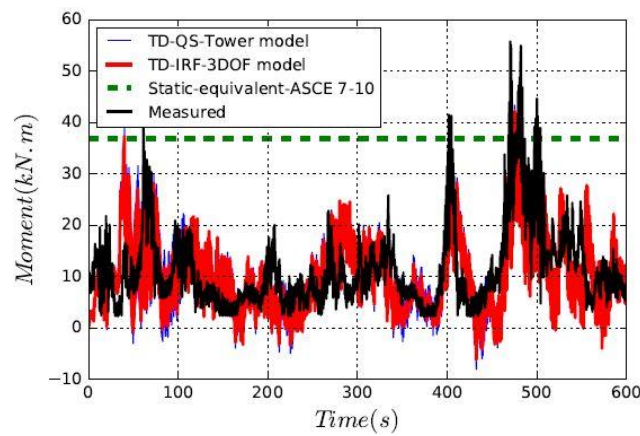
(a) Typical example at  $\gamma=0^\circ$ (b) Typical example at  $\gamma=90^\circ$ 

Fig. 4 Measured and simulated base moment time history of for different models

Table 1 Relative error for statistical parameters for IRF method using the two models compared to the experimental results

Event	$V_m$	$I_u$	Measured			Tower model			3 DOF- model		
			$M_0$	$M_{0max}$	$\sigma_0$	$M/M_0$	$M_{max}/M_{0max}$	$\sigma/\sigma_0$	$M/M_0$	$M_{max}/M_{0max}$	$\sigma/\sigma_0$
1	7.54	0.34	21.50	79.98	15.00	0.83	0.99	1.06	0.85	1.02	1.12
2	6.55	0.37	14.50	76.90	10.72	0.86	0.64	0.89	0.89	0.62	0.93
3	7.55	0.30	17.40	72.71	11.09	0.89	0.67	0.88	0.93	0.74	0.94
4	6.11	0.33	11.40	55.70	17.99	0.88	0.75	0.84	0.92	0.77	0.88
5	8.03	0.30	21.30	76.71	2.37	0.87	0.99	1.61	0.86	1.04	1.41
6	6.37	0.29	18.34	63.66	9.14	0.85	1.23	1.25	0.84	1.16	1.18
7	7.32	0.35	14.31	60.66	7.68	0.87	0.84	1.32	0.85	0.78	1.15
8	6.62	0.31	10.80	39.46	3.65	0.88	1.18	1.71	0.86	1.09	1.49
9	6.59	0.27	15.06	47.75	6.07	0.91	0.92	1.16	0.89	0.90	1.06
10	6.79	0.29	17.01	51.02	10.10	0.86	1.14	1.31	0.86	1.15	1.28
E	6.79	0.64	15.99	61.77	9.38	0.87	0.94	1.20	0.88	0.93	1.14
$\sigma_E$	0.31	0.03	8.00	21.12	0.02	0.86	0.20	0.29	0.02	0.19	0.20

values. Table 1 shows the comparison results for 10 representative test samples at pitch angle  $\gamma=90^\circ$  for both the intermediate tower model and the 3-DOF model. In Table 2, the frequency domain methods and the time-domain method (IRF) applied to the 3-DOF model are also compared for the same typical tests in term of adimensional parameters, the response turbulence  $I_r$  and the GEF. The

ratios between simulated and measured values are calculated for each test and E represents the average of these ratios over all tests.  $\sigma_x$  is the standard deviation for this ratio. Fig. 4 also presents the time history analysis comparison for two typical test samples of the two models compared to full-scale measurements at two pitching angle  $\gamma=0^\circ$  and  $\gamma=90^\circ$ .

Table 2 Comparison between the calculated statistical parameters from the measured and simulated base moment using different methods

Event	Measured		ASCE7-10		Spectral approach		3 DOF- model	
	$I_r$	GEF	$I_r$	GEF	$I_r$	GEF	$I_r$	GEF
1	0.53	0.79	0.96	1.22	1.04	0.91	0.92	1.16
2	0.71	1.12	0.80	0.86	1.04	0.69	0.80	0.71
3	0.64	1.27	0.70	0.80	0.85	0.66	0.84	0.82
4	0.70	0.97	0.69	0.93	0.74	0.75	0.88	0.84
5	0.37	1.18	1.08	0.88	1.20	0.80	1.23	1.09
6	0.43	0.92	1.02	0.98	0.90	0.79	1.01	1.01
7	0.54	0.94	0.90	1.04	1.21	0.73	1.01	0.91
8	0.40	1.07	1.06	0.88	1.00	0.64	1.31	1.06
9	0.46	0.94	0.82	0.99	0.96	0.98	0.94	1.14
10	0.37	0.84	1.10	1.17	1.23	1.01	1.10	1.19
E	-	-	0.91	0.98	1.02	0.80	1.01	0.99
$\sigma_E$	-	-	0.15	0.13	0.16	0.12	0.17	0.16

Figs. 4(a) and 4(b) shows that the dynamic response of the CPV prototype using the indicial response function (IRF) contribute to approach the maximum and RMS values of the full-scale response. However, it seems to be difficult to match the time history and predict all peak occurrence. Other fluid flow phenomenons, such us vortex shedding, which may supposed to occur at relatively low frequency range for the low wind speed conditions for this CPV prototype, may contribute to understand the complete temporal sequence of the measured global moment at the base. In general, despite of the common difficulty related to modeling the fluid flow and with only considering the along wind response, the proposed time-domain method could predict the important measured response peaks in its deterministic occurrence and the total background response with relatively acceptable variation. It is also shown that the time history of both the simplified and the complete model are similar, which validates the use of the 3-DOF model for the parametric study. It is also important to notice that the commonly used quasi-steady approach, which was simulated but not presented in the figures, highly overestimate the measured peaks compared to the IRF approach.

Table 1 shows that overall, the time-domain method with the adopted IRF model is successful to predict the statistical wind response parameters. The maximum and the standard deviation are predicted with statistical average ratios E of 0.93 and 1.14, and with statistical dispersion  $\sigma_E$  of 0.19 and 0.20, respectively. The mean wind response of the IRF method is slightly underestimated due to the linearized form of the applied wind force which neglects the turbulence second term. This contribute to slightly underestimate the measured peak values  $E=0.93$ . However, as shown in Table 2, by comparing the gust effect factor and the response turbulence the prediction error decrease to  $E = 0.99$  and  $E=1.01$  because of their normalized form with respect to the mean response (Kaabia *et al.* 2017b). Table 2 shows also a good agreement and similar results between time-domain analyses based on the IRF, the spectral approach and the ASCE 7 formulation. Relatively more important variation is observed for the spectral approach results. The resonance peak factor  $g_r$  ( $T=600s$ ), based on a

probabilistic basis (Rayleigh distribution), is evaluated to 4.2 or 4.5 depending on considering the pitching or the swaying frequency. Then, many test records showed measured response peak factor  $g$ , associated to serviceability low wind speed conditions, to be higher than the analytical value range (2.1-5) (Eq. (10)). This could contribute in slightly underestimating the peak values for the study of loading cases for weak and moderate wind speed conditions. The SRSS method used to predict the maximum response as a combination of the peak caused by the drag force and the pitching moment could also explain a part of dispersion of the results between the frequency and the time-domain approaches. The algebraic combination (AC) could reduce this variation and it is used for the parametric study.

It is then concluded that, the time-domain method applied to the 3-DOF model could be confidently used to extend the numerical investigation for design conditions in order to test many study cases as described below and then identify optimal structural design alternatives regarding wind load actions.

### 3.2 Parametric study

The parametric study is conducted for many structural and wind parameters and results are grouped and discussed as follows:

#### Structural parameters

Figs. 5(a)-5(c) show the effect of the main structural dynamic parameters, including the pitching and swaying frequencies and the damping ratio, on the dynamic wind response. The gust effect factor is selected to study this effect. In these figures, the dynamic contribution in the total response is highlighted in a lighter hatched color. For the time-domain method, the dynamic contribution part is calculated as a difference between the results from the total dynamic response and the response issued from a static incremental analysis using the time depending wind loading. For the frequency domain method, it is simply the difference between the results with dynamic and static hypotheses. Only the results of high reference wind speed

( $V_m=30$  m/s) at stow position ( $\gamma=90^\circ$ ) are shown in the bar presentation. In the same plot, the results are also compared to the ASCE 7-10 and the modified ASCE 7-10-AC and the spectral approach using the algebraic combination method. Figs. 5(d) and 5(e) summarize the gust effect factor variation, issued from the numerical time-domain method, after varying the pitching and swaying frequencies at different pitch angles and different mean wind speed values.

According to Fig. 5(c), the wind dynamic response is highly sensitive to the structural damping for high wind speed. The peak response could be reduced by 30% by improving the reference structural damping to 2%. Therefore, a cost effective study for improving the damping characteristics of this type of structure is recommended. Similarly, the peak wind response could be reduced by a maximum of 35% and 20%, by varying the pitching and the swaying frequencies in the range of [0.4-1.6] Hz and [1.5-5.3] Hz, respectively (Figs. 5(a) and 5(b)). Particularly for this type of structure at the stow position, along-wind drag resonance would be less important due to the role of the admittance function in attenuating the correlation between wind speed and exercised forces at high frequency range. However, the first eigenfrequency, which is usually the pitching frequency, exhibit more significant energy. Therefore, in practice, it is aimed to increase the first eigenfrequency in order to avoid highly vulnerable range to resonance ( $\sim 1.2$ ). Fig. 5(d) shows that the variation of the *GEF* becomes smoother from 1.2 to 1.6 Hz. Thus, more attention might be taken in controlling the stiffness of the dish support frame as well as the flexibility of the rotational elevation mechanism for this type of structure. It is also important to maintain relatively stiff support tower structure to guarantee a swaying frequency range higher than 3 Hz in order to reduce to minimum the dynamic vibration which may be not favorable for operational configurations where drag force would be more important (Fig. 5(e)). At the same time, it is unnecessary to reach more important frequency ranges which could led to non economic steel configurations. Usually the lowest frequency of such type of structures is higher than 1 Hz such as the typical heliostat prototypes studied by Sandia Laboratory (Griffith *et al.* 2014). This condition is favorable to get acceptable dynamic amplification and it could be improved depending in economic considerations.

In figures Figs. 5(d) and 5(e), the study of the frequency effect is extended to different loading cases. It is shown that particularly for this type of structure, the stow position is the most vulnerable to the dynamic effect at high wind speed conditions for all frequency ranges, even though the drag wind force is at its minimum. At this position, the low frequency exhibits more significant energy due to the important pitching moment, which is not the case of the other positions. At service conditions  $V=7$  m/s, only relatively small dynamic amplification could occur and it might be controlled in order to ensure the target optical efficiency.

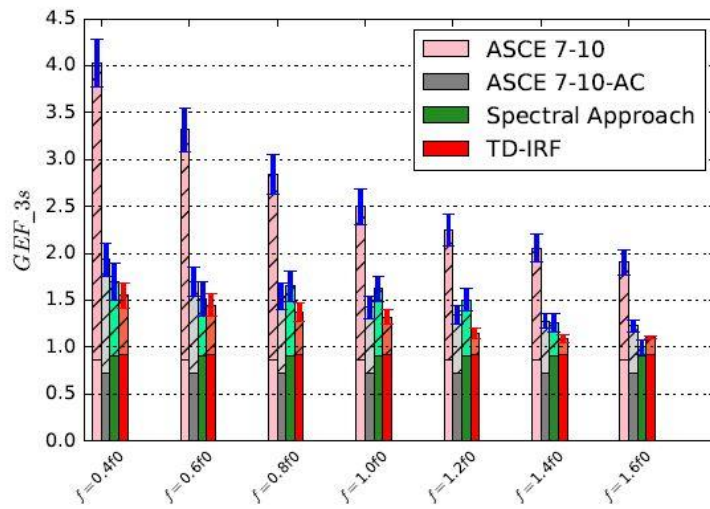
For a comparison and in order to maintain coherence with standard frequency approaches, the analysis was also made for the ASCE 7-10 and Davenport's spectral approach. Overall, the percentage of variation according to the studied

parameters are similar. All the methods show close values for the background response. A relatively small difference between the IRF and the spectral approach compared to the ASCE 7-10 could be related to the additional hypothesis of spatial correlation adopted for the ASCE 7-10 as well as the relatively different aerodynamic admittance function. Unlike the background component, important discrepancies are observed for predicting the resonant part compared to the ASCE 7-10. The major part of the variation is due to the consideration of only the contribution of the first frequency to the resonant response in applying the *GEF* concept according to the ASCE 7-10. This assumption seems to be conservative because it does not include the participation of the second mode shape that could attenuate the normalized dynamic effect regarding the mean wind response. This assumption seems to lead to high variation for higher wind speed scenarios, which is clearly less observed for lower wind speed range, where the dynamic part is less sensible (Table 2). Then, in practice it seems to be important to combine the probable peaks coming from the two mode excitation using the algebraic combination (AC) in calculating the maximum response due to the pitching moment and the drag force in order to get more coherent results (Figs. 5(a)-5(c)). The discrepancies with the other methods would be only due to the aerodynamic admittance form and the non-considered possible dynamic interaction effect between the two mode shapes which is not considered in the frequency approaches.

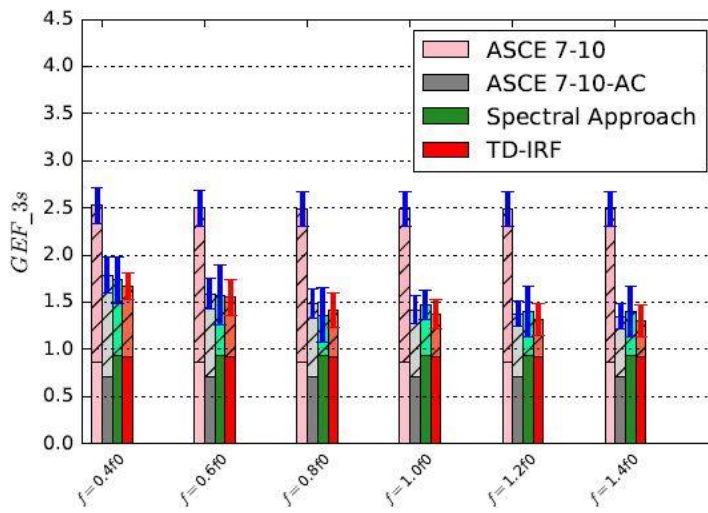
#### Wind parameters

In this study, the peak wind response of the reference prototype is evaluated for various wind design speed at different locations for different configurations (Fig. 6(a)). The applied design wind speed values are the 3-s gust wind speed as predicted in ASCE 7-10 for a risk category II and for wind return period of 50 years. The selected wind speeds correspond to different locations in the USA (Arvada-CO, Dateland-AZ, Miami-FL, Hawaii) with different wind characteristics where many solar plants were installed. Fig. 6(b) presents also the effect of changing the site exposure category hypothesis according to the ASCE 7-10 process. The site categories are varied for a reference location situated at 115 mph basic wind speed contour (51 m/s) (ASCE 7-10 wind speed map). Then, the corresponding mean wind speed and the turbulence intensity used for generating wind samples for each site category are calculated using the Terrain Exposure Constant Table in ASCE 7-10. The study is applied to the reference CPV prototype.

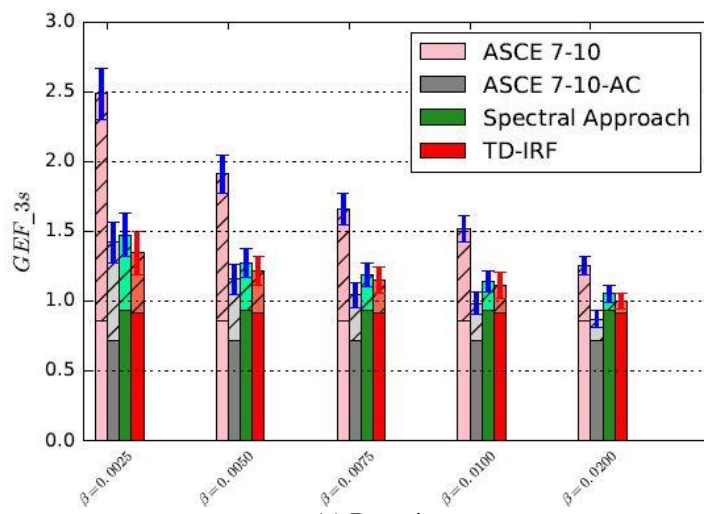
The peak wind response is highly dependent on the location. As shown in Fig. 6(a), the calculated design wind load could be more than four times higher for the special wind region ( $V_m=55$  m/s) compared to the moderate wind speed region ( $V_m=30$  m/s). In the same figure, it is also shown, that the movable aspect of this type of structure is advantageous to optimize the wind load calculation at ultimate state.



(a) Pitch frequency



(b) Sway frequency



(c) Damping

Continued-

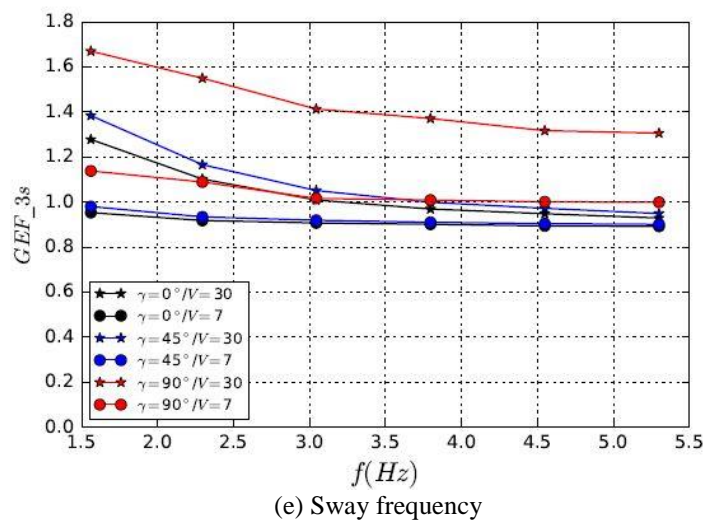
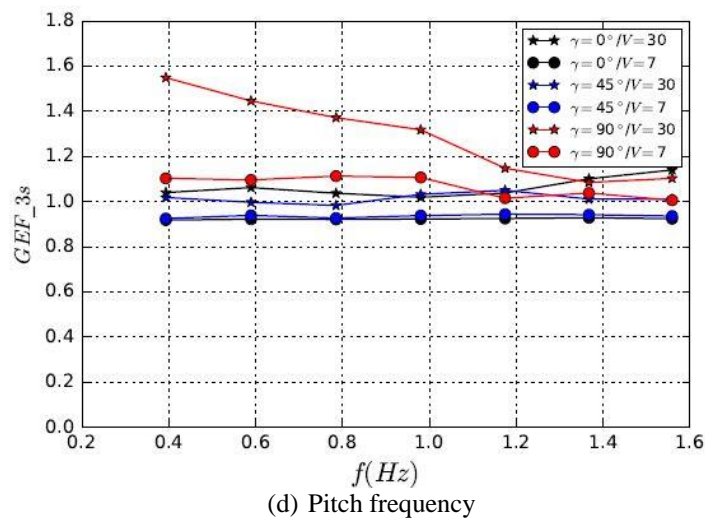


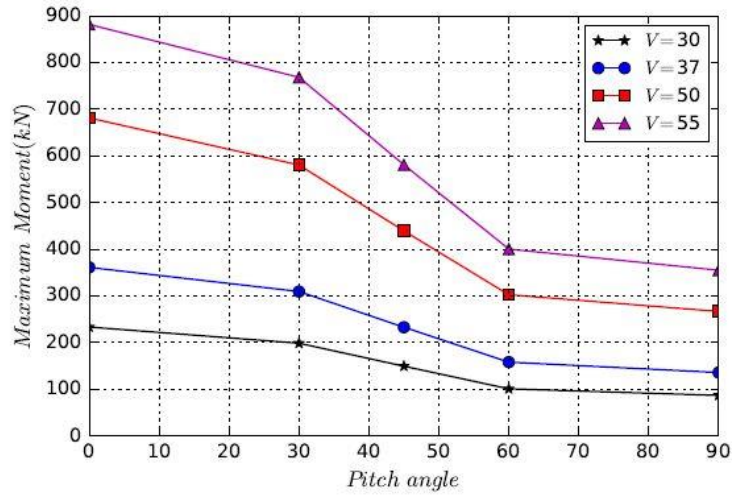
Fig. 5 Effect of structural parameters on gust effect factor

The design peak wind load might be considered only for stow position at  $\gamma = 90^\circ$  even though an important dynamic amplification could occur as discussed in the precedent section. Then, designers should pay more attention to the dynamic amplification due to the pitching frequency at this particular position. For example, for the reference location and the reference site category, the dynamic part could reach 33% of the total response for this angle compared to only 5% for  $\gamma = 0^\circ$ . Fig. 6(b) shows that the topography profile and surface roughness of the system site could highly influence its design wind loads. For example, at the reference location, the peak wind load for a site type D is estimated to be two times compared to the value for the reference exposure category B. The corresponding dynamic effect is also relatively higher. Fig. 6(c) also shows that the peak response increase rapidly with the turbulence intensity. The maximum variations between low (13%) and high (40%) turbulence intensity could reach 52%, 49% and 42% for the tested mean wind speed of 19, 30, 44 m/s related to different exposure categories for the reference location, respectively.

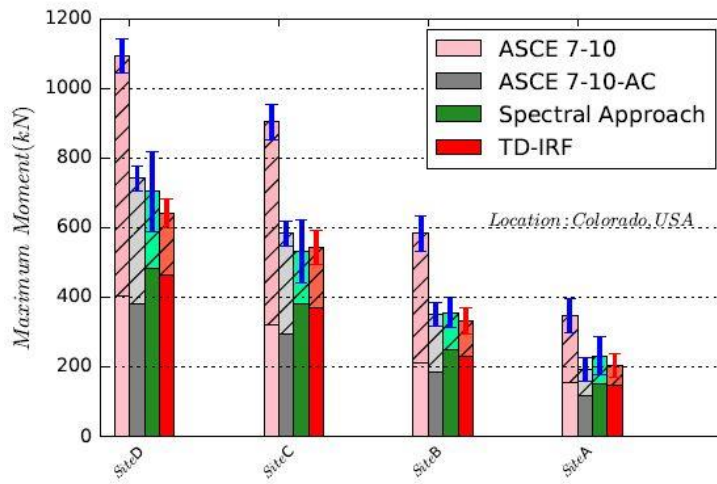
It is concluded that wind dynamic action might be considered in addition to the common parameter of the annual insolation, in selecting the location of the solar plant. It is shown that wind response for design and operational conditions are significantly depending on the site and it is highly recommended to adapt the prototype to the specific location where it would be commercialized in order to meet cost effective design objectives. Site wind measurement are also highly recommended in order to get optimized wind load evaluation.

#### Geometric parameters

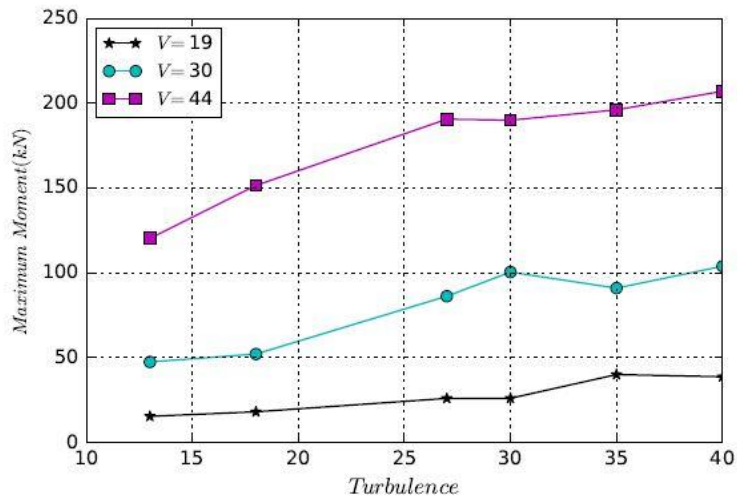
The sizing of the dish collector is a key parameter that controls simultaneously the structural design and the optical capacity. In this paper, new prototype configurations are tested by varying the dish collector area size and its aspect ratio. It is considered that the pivot height of the support structure and the initial geometry of the reference support structure prototype are maintained unchanged. The study is conducted for design conditions at stow position.



(a) Locations



(b) Site category



(c) Turbulence intensity

Fig. 6 Effect of wind parameters on peak wind response for the reference CPV prototype

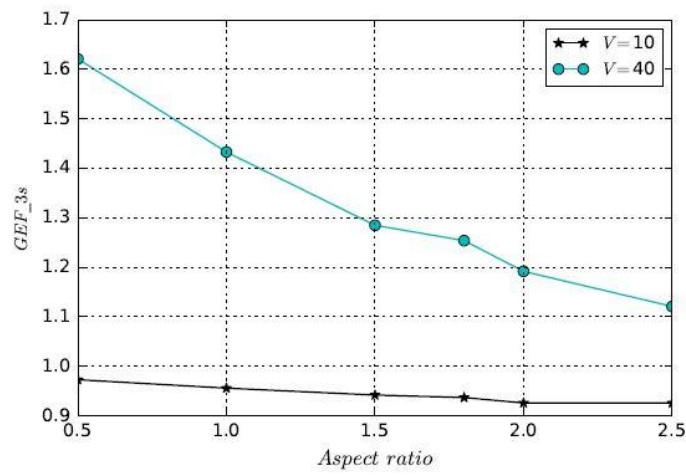
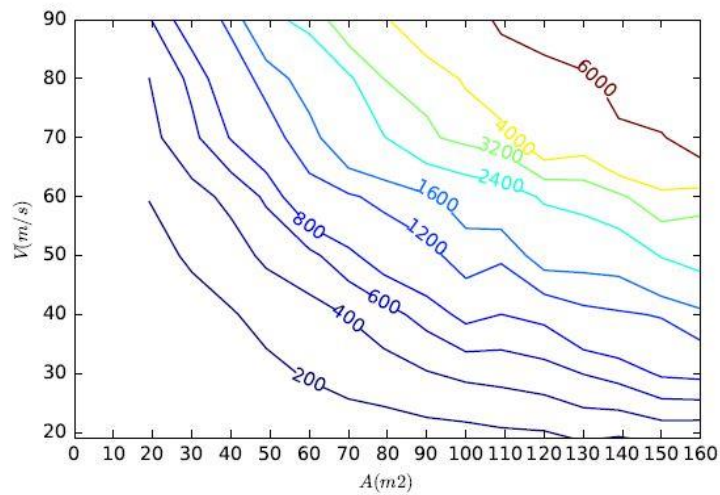
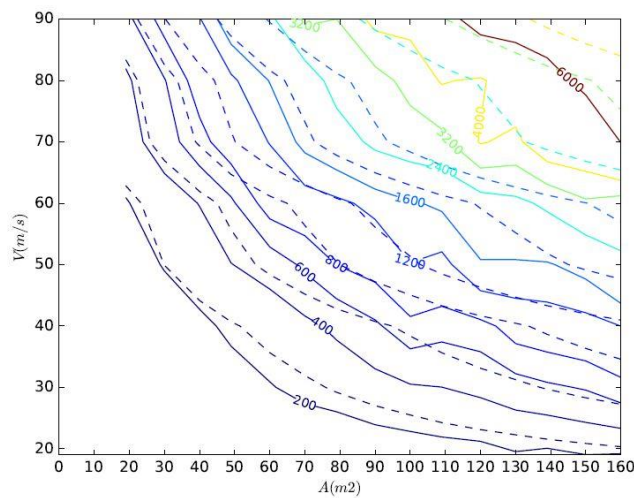


Fig. 7 Variation of gust effect factor as a function of aspect ratio

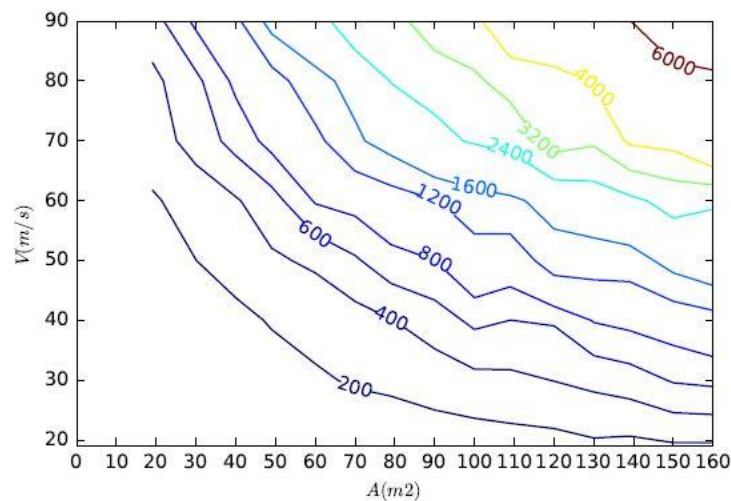


(a) Aspect ratio=1.0



(b) Aspect ratio=1.8

Continued-



(c) Aspect ratio=2.5

Fig. 8 Peak dynamic response as a function of wind speed and tracker area for selected aspect ratio

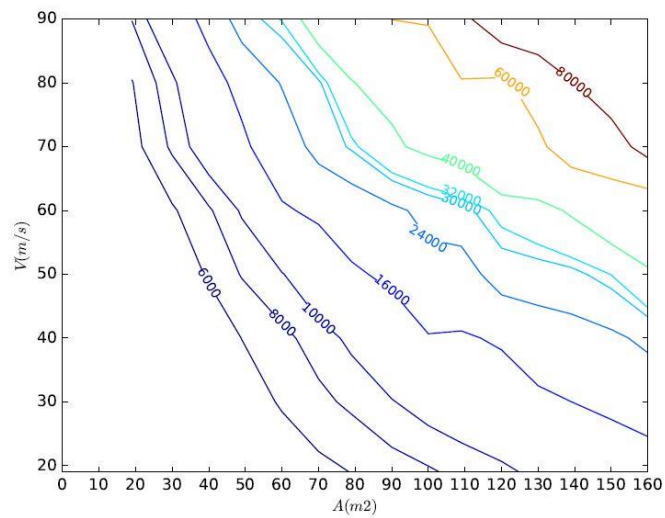
Fig. 7 shows the variation of the gust effect factor and the dynamic effect in function of the aspect ratio for the stow position at two different wind speed for service and ultimate conditions. Theoretically, aerodynamic coefficients may change with the aspect ratio. Here, the variation of the mean force and moment coefficients are proportionally adjusted based on the study (Griffith *et al.* 2014). In addition to that, changing the aspect ratio also change the chord length of the dish. Then, it is confirmed, from Fig. 7, that more the aspect ratio is important, which is equivalent to smaller panel chord length, more the wind design force case is optimized for the same area size. This variation is also more noticeable for high wind speed conditions.

Fig. 8 shows a more detailed analysis including many combinations of wind speed and dish collector size area for three aspect ratio values 1.5, 1.8 and 2.5. The variation of the force and moment coefficient for this range and for the pitch angle  $\gamma = 90^\circ$ . However, considering only the variation of the effective lever arm or the chord length of the panel, the peak wind response may significantly change for this stow position where the pitching moment is important. Then, it can be confirmed, from Fig. 8, that the expected wind loads vary significantly with the aspect ratio of the tracker for different wind speed and area size configurations. Peak wind load values are more important for trackers with smaller aspect ratios for a selected area size and wind speed. For example, for the design of a CPV prototype having a dish collector area of  $100 \text{ m}^2$  at design wind speed of  $40 \text{ m/s}$ , the design peak wind response could vary from  $600$  to  $700$  and to  $800 \text{ kN.m}$  for the aspect ratios of 2.5, 1.8 and 1.0, respectively. Potential reduction of 33% could be relatively achieved without changing the optical capacity. Then, the structure prototypes with higher aspect ratio are lighter for the same dish area size. Indeed, the larger the aspect ratio is, the smaller the pitching moment dynamic action becomes. This variation according to the aspect ratio become more critical for higher design wind speed and higher dish area size scenarios.

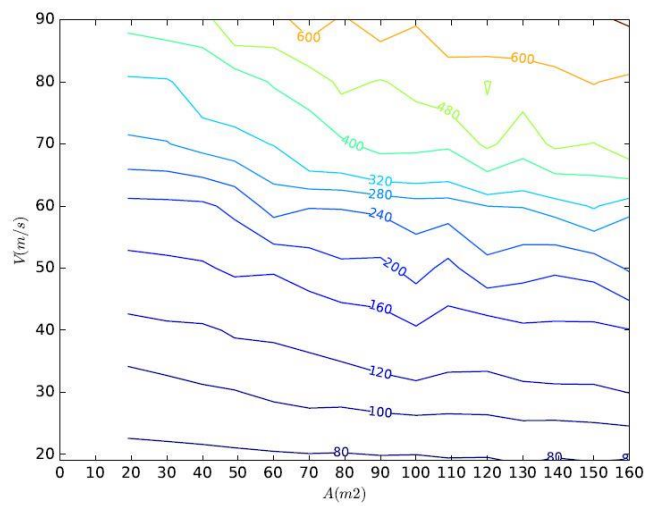
Fig. 8(b) also superposes the results of the time-domain dynamic analysis and the results of the incremental static analysis in dashed line. It is shown that the wind peak response calculated with static assumption may underestimate the response for all the area size and wind speed. In preliminary design, the calculated mean wind speed assumed a static behavior lead to non-conservative design. For example, designing a CPV prototype with a surface of  $100 \text{ m}^2$  under design wind speed of  $40 \text{ m/s}$  at the reference site wind conditions using static hypothesis, is equivalent to designing the same prototype with lower wind speed of  $30 \text{ m/s}$  by considering the dynamic effect. This non-conservative indication could be amplified for the higher wind speed and higher area size configurations.

#### *Steel weight of the support tower*

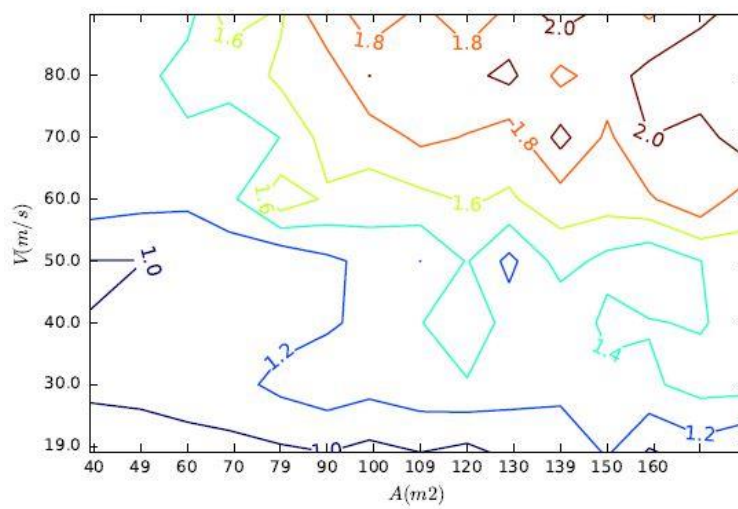
The following analysis deals with a preliminary design benchmark exercise for the support tower structure principal members. Due to the wind force and the self-weight of the structure, tensile and compression forces would be monitored to the principal six L section members in order to withstand the experienced forces (Fig. 1). Then, new steel weight of the updated configuration to withstand the peak wind loads and the gravity loads is calculated. Many design simplification hypotheses are taken in order to focus more specifically on the global aspect of the effect of the dynamic action on the structure cost in general. First, the mass of the dish collector is updated proportionally to the area size variation. Second, the design of the tower support principal members consists on resizing the section in function of the new calculated wind loads and self weight in order to get the same percentage of axial stresses as for the initial design of the reference prototype. The percentage values of admissible stress associated to the six members were estimated for the reference prototype at design wind speed value ( $V=40 \text{ m/s}$ ) by using static analysis. Then, it should be also noted that this hypothesis could not lead to



(a) Mass (kg)



(b) Normalized mass (kg/m<sup>2</sup>)



(c) GEF

Fig. 9 Wind load and mass specification as a function of wind speed and tracker area

the most optimized configuration but it provides an important reference to compare coherently the global tendency of the variation in function of the studied parameters. Finally, the total mass is calculated as a summation of the dish collector mass and the tower support principal members mass.

Fig. 8(b) shows the calculated peak wind response as a function of wind speed and tracker area. The dynamic amplification is presented with the parameter  $GEF$  in Fig. 9d. The required amount of steel mass (Fig. 9(a)) and normalized steel mass in  $\text{kg}/\text{m}^2$  (Fig. 9(d)) to withstand the calculated wind force are calculated from the wind response from Fig. 8(b) using the explained process.

Fig. 9 shows that for a selected design wind speed value, the maximum wind response and the variation of the mass of the steel support structure are not linear with the variation of the area size contrary to what is expected by the static analysis. At higher wind speed, the sensitivity of the mass and the normalized mass in  $\text{kg}/\text{m}^2$  to the variation of the area become more critical (Figs. 9(a) and 9(b)). This result is in concordance with the observed variation of the  $GEF$  parameter in Fig. 9(c), where the dynamic effect is amplified for these critical zones  $GEF \geq 1$ .

Fig. 9 shows also that when the wind speed value becomes higher than  $V=30$  m/s, it would be more disadvantageous to increase the collector area size for high wind speed because the added support steel mass in  $\text{kg}/\text{m}^2$  would be more important. For example, when  $V=20$  m/s, overall the normalized required mass is evaluated to  $80 \text{ kg}/\text{m}^2$  for all the size area (Fig. 9(b)) because the probable dynamic effect is relatively small  $GEF < 1$  for all scenarios (Fig. 9(c)). However, for a higher wind speed values, for example for  $V=60$  m/s, the increase of the size area from  $100 \text{ m}^2$  ( $200 \text{ kN}/\text{m}^2$ ) to  $140 \text{ m}^2$  ( $240 \text{ kN}/\text{m}^2$ ) would rapidly increase the cost of a  $\text{m}^2$  capacity by  $\sim 20\%$  (Fig. 9(b)). Then, it is important to pay attention that the gain in optical capacity could be constrained by the dynamic amplification caused by wind action depending on wind speed values. Designers could roughly use or easily reproduce these plots for similar structures in order to evaluate different design configurations with considering the dynamic amplification which could be critical and led to non-economic alternatives.

#### 4. Conclusions

The present parametric study permit to evaluate the effect of the structural parameters and wind site specifications on the dynamic wind load response and then on the steel support structure weight. The study is based on a developed time-domain method, which is validated for full-scale experimental results for the studied reference CPV prototype. The parametric study leads to the following general conclusions concerning the design of steel support structure of solar systems in general:

- Time-domain analysis using simplified structural model and indicial function approach for flat plate could coherently predict design wind load for

similar CPV structure geometry with acceptable variation;

- Considering only the static analysis to calculate solar structure response under wind loads could lead to nonconservative design for steel support structure. The dynamic effects of gusts on the concentrator wind loads, induced especially by the pitching moment at the stow position, is important for this type of flexible structures;
- Reduction of aerodynamic wind loads for the same optical capacity is possible in practice by increasing the aspect ratio, improving the structural damping, controlling the flexibility of the elevation and azimuthal mechanism and avoiding the vulnerable frequencies ranges;
- Wind conditions are highly site specific. Thus, accurate identification of the site wind characteristics is recommended. Reliable wind measurements close to a selected site are desirable and flexibility to take into account various uncertainties in wind characteristics is also a key parameter to optimal structural design;
- The dish collector area size selection may go further than the optical capacity. Wind dynamic action could represent a constraint to get a cost-effective steel mass ( $\text{kg}/\text{m}^2$ ). In some cases, adding the area could highly increase the additional weight of the structure in  $\text{kg}/\text{m}^2$  of optical surface. Then, the evidence of the relationship between collector area and cost is biased if it does not account for the dynamic wind action;
- Further investigations are necessary in order to propose recommendations taking into consideration the total cost and the optical quality for this structure to get the lowest cost of energy for this type of structure.

#### Acknowledgments

The authors would like to thank SpaceWatts division of Gestion TechnoCap for the technical contributions and financial support for the research, along with NSERC, PROMPT and Hydro-Sherbrooke. We are also grateful for the financial contributions of the Canadian foundation for Innovation (FCI), the Ministère de l'Économie, Science et Innovation of Québec and the Université of Sherbrooke for the unique CPV infrastructures. Finally, the technical contribution of M. Richard Norman for the work related to the CPV prototype is greatly acknowledged.

#### References

- ASCE7-10 (2010), "Minimum design loads for buildings and other structures", ASCE, Reston, VA.

- Banks, D. (2012), How wind load studies will impact the solar industry”, *Tech. rep.*, CPP, Inc, Fort Collins, CO. USA.
- Chang, B. (2010), “Time-domain model for predicting aerodynamic loads on a slender support structure for fatigue design”, *J. Eng. Mech.*, **136**(6), 736-746.
- Chen, X. and Kareem, A. (2002), “Advances in modeling of aerodynamic forces on bridge decks”, *J. Eng. Mech.*, **128**(11), 1193-1205.
- Davenport, A. (1961), “The application of statistical concept to the wind loading of structures”, *Proceeding of the Institution of Civil Engineers*, **19**(4), 449-472.
- Davenport, A. (1967), “Gust loading factors”, *J. Struct. Div., ASCE*, **93**(3), 11-34.
- Fu, W., Yang, M.C., Zhu, Y.Z. and Yang, L. (2015), “The wind-structure interaction analysis and optimization of parabolic trough collector”, *Energ. Procedia*, **69**, 77-83.
- Gani, F. and Lègèron, F. (2010), “Dynamic response of transmission lines guyed towers under wind loading”, *Cand. J. Civ. Eng.*, **37**, 450-464.
- Gani, F., Lègèron, F. and Norman, R. (2011), “Refinement of design for parabolic truss structure for solar concentrating photovoltaic tracker system”, *Proceeding of the Annual conference of the canadian society of civil engineering*, Ottawa, May.
- Giannuzzi, G.M., Majorana, C.E., Miliozzi, A., Salomoni, V.A. and Nicolini, D. (2007), “Structural design criteria for steel components of parabolic-trough solar concentrators”, *J. Solar Energ. Eng.*, **129**(4), 382-385.
- Gil, A.M., Acin, A., Rueda, F. and Mayor, I. (2009), “Structural and motion system dynamic analysis of a two-axes solar tracker under wind action”, *Proceeding of the Simulia customer Conference*, London, May.
- Griffith, T.D., Moya, A.C., Ho, C.K. and Hunter, P.S. (2014), “Structural dynamics testing and analysis for design evaluation and monitoring of heliostats”, *J. Solar Energ. Eng.*, **137**(2), 210-223.
- Hang, S.G.F. and Lègèron, F. (2005), “WindGen, Générateur de vent appliqué au génie civil”, *Tech. Rep.* Université de Sherbrooke.
- Hosoya, N., Peterka, J.A., Gee, R.C. and Kearney, D. (2008), “Wind tunnel tests of parabolic trough solar collectors”, *Tech. rep.*, National Renewable Energy Laboratory, Colorado, US.
- Kaabia, B., Langlois, S. and Lègèron, F. (2017a), “Full-scale measurement of the response of a CPV tracker structure prototype under wind load”, *J. Solar Energ.*, **147**, 368-380.
- Kaabia, B., Langlois, S., Maheux, S. and Lègèron, F. (2017), “Time-domain analysis of solar concentrator structure under gust wind”, *Proceeding of the 13th Americas Conference on Wind Engineering (13ACWE)*, Gainesville, May.
- Letchford, C.W., Iverson, R.E. and McDonald, J.R. (1993), “The application of the quasi-steady theory to full scale measurements on the texas tech building”, *J. Wind Eng. Ind. Aerod.*, **48**(1), 111-132.
- Murphy, L.M. (1981), “An assessment of existing studies of wind loading on solar collectors”, *Tech. rep.*, Solar Energy Research Institute, Colorado, US.
- Norman, R., Dauphin, P. and De St. Croix, F. (2010), “Systems for cost effective concentration and utilization of solar energy”, WO2010118503.
- Peterka, J.A., Sinou, J.M. and Cermak, J.E. (1980), “Mean wind forces on parabolic-trough solar collectors”, *report sand 80-7023. Tech. rep.*, Sandia National Laboratories, Colorado, US.
- Pfahl, A., Buselmeier, M. and Zschke, M. (2011), “Wind loads on heliostats and photovoltaic trackers of various aspect ratios”, *J. Solar Energ.*, **85**(9), 2185-2201.
- Randall, D.E. (1983), “Correlations of solar insolation and wind data for solmet”, *J. Solar Energ. Eng.*, **105**, 168-173.
- Salomoni, V.A., Majorana, C., Giannuzzi, G. and Miliozzi, A. (2009), “Structural design of parabolic-trough solar concentrators”, *J. Solar Energ. Eng.*, Dipmat.Univpm.It, **388**, 382-390.
- Scanlan, R.H. (1993), “Problematics in formulation of wind force models for bridge decks”, *J. Eng. Mech.*, **119**(7), 1353-1375.
- Vickery, B. (1968), “The application of statistical concept to the wind loading of structures”, *J. Eng. Mech. Div. - ASCE*, **94**(1), 31-46.
- Wu, Z., Lei, D., Yuan, G., Shao, J., Zhang, Y. and Wang, Z. (2014), “Structural reliability analysis of parabolic trough receivers”, *J. Appl. Energ.*, **123**, 232-241.
- Zlatanov, H. and Weinrebe, G. (2013), “CSP and PV solar tracker optimization tool”, *Energ. Procedia*, **49**, 1603-1611.

AD